JMEPEG (2018) 27:1635–1641
https://doi.org/10.1007/s11665-018-3250-9

1059-9495/$19.00

Electrochemical Behavior of Biomedical Titanium Alloys Coated with Diamond Carbon in Hanks' Solution

S. Gnanavel, S. Ponnusamy, L. Mohan, R. Radhika, C. Muthamizhchelvan, and K. Ramasubramanian

(Submitted May 18, 2017; in revised form November 24, 2017; published online March 8, 2018)

Biomedical implants in the knee and hip are frequent failures because of corrosion and stress on the joints. To solve this important problem, metal implants can be coated with diamond carbon, and this coating plays a critical role in providing an increased resistance to implants toward corrosion. In this study, we have employed diamond carbon coating over Ti-6Al-4V and Ti-13Nb-13Zr alloys using hot filament chemical vapor deposition method which is well-established coating process that significantly improves the resistance toward corrosion, wears and hardness. The diamond carbon-coated Ti-13Nb-13Zr alloy showed an increased microhardness in the range of 850 HV. Electrochemical impedance spectroscopy and polarization studies in SBF solution (simulated body fluid solution) were carried out to understand the in vitro behavior of uncoated as well as coated titanium alloys. The experimental results showed that the corrosion resistance of Ti-13Nb-13Zr alloy is relatively higher when compared with diamond carbon-coated Ti-6Al-4V alloys due to the presence of β phase in the Ti-13Nb-13Zr alloy. Electrochemical impedance results showed that the diamond carbon-coated alloys behave as an ideal capacitor in the body fluid solution. Moreover, the stability in mechanical properties during the corrosion process was maintained for diamond carbon-coated titanium alloys.

Keywords corrosion, diamond carbon, electrochemical impedance, HFCVD, titanium alloys

1. Introduction

Orthopedic implants like hip and knee joint replacements are important to clinicians. Before 2030, the enthusiasm of knee and hip joint replacement system is foreseen to create by 674 and 172% independently, in the USA alone (Ref 1). Inferable from these requests, the life hope of the implants is of vital significance and anticipated that would serve for a more extended period. Now, the industrial metallic materials are utilized for the orthopedic implants (titanium alloys, Co-Cr compounds and 316 L stainless steel-based combinations) and fail within 16-24 years which thus prompts amendment surgery. In 2030, knee and hip replacement update operation would rely upon an increment of 135% and 600%, respectively. Therefore, it is highly necessary to increase the corrosion and mechanical properties of an implant by coating. If that happened, the patient would stay away with unwanted pain from the correction surgery (Ref 2-4).

The primary purpose behind the failure of implants is due to the generation wear fragments and metal molecule release from the bearing surface during the wear and corrosion process which in turn induces osteolysis and results in aseptic discharging of orthopedic implants (Ref 5). It is seen that articulating movement of hip and knee replacement affects the sliding contact in a corrosive biological environment, hence by making the implant subjected to corrosion and wear resistance simultaneously. It is essential to say that titanium alloys have good corrosion resistance; however, under the stress and strain effect, they show the corrosion rates (Ref 6). Yan et al. (Ref 7) showed that 20-30% material loss in Co-Cr alloys was due to the corrosion mechanism which is generally reacted in the hip implant (femoral head).

α-β and near-β titanium alloys found the wide applications in biomedical implants in both load bearing and non-load bearing joints, due to their superior mechanical strength and excellent biocompatibility (Ref 8). The titanium alloys utilized as implants are reasonable because it is nontoxic and does not allow any opposite reaction in the biological tissue (Ref 9). At room temperature conditions, titanium combinations are classified as α, near α, α + β, metastable β and near β. Among the various β combinations, near-β alloy Ti-13Nb-13Zr is found to be more appropriate for implant work because of less elastic modulus and contains the simple combination of the elements such as Zr and Nb (Ref 10). Furthermore, Ti-6Al-4V was mostly used for artificial bone joints replacements because of its high hardness. Unlike chemical reactions, corrosion of the metal implants results in the degradation of implants. Thus, the degradation of implants due to corrosion may cause a local inflammatory response, and it may lead to the following: cessation of bone formation, synovitis and detachment of artificial implants (Ref 11).

On the other hand, the low wear resistance of implants induces the wear debris formation. There may be several reactions to occur in tissues due to the small wear resistance which leads to increase the possibility of implants failure. Thus, the mechanical properties of implants are highly relevant, and it depends on material volume and its surface characteristics (Ref

S. Gnanavel, Department of Biomedical Engineering, SRM Institute of Science and Technology, Chennai, Tamilnadu, India; **S. Ponnusamy** and **C. Muthamizhchelvan**, Centre for Materials Science and Nano Devices, SRM Institute of Science and Technology,, Chennai, Tamilnadu, India; **L. Mohan**, Surface Engineering Division, CSIR-National Aerospace Laboratories, Bangalore, India; and **R. Radhika** and **K. Ramasubramanian**, Nano Functional Materials Technology Centre, Indian Institute of Technology Madras, Chennai, India. Contact e-mails: gnanambe06@gmail.com and suruponnus@gmail.com.

12, 13). To prevent the corrosion of metallic implant and improve the bioactivity, there is a need for proper surface modification of metallic implants which can be achieved through the deposition of various functional coating materials. To promote the corrosion and wear resistance of implants, two ways are usually followed, such as (1) ''bulk alloying'' and (2) ''surface modification.'' In this study, we have focused on surface modification of implants to solve the aforementioned problems for the biological implant applications (Ref 14). There are various metal implant surface modification techniques reported in the literature; among them, surface modification using ''diamond carbon-coated'' called DCC is found to be an excellent method because of its good mechanical properties (high hardness), chemical, biological inertness and makes it suitable for biomedical implant application (Ref 15, 16). DCC has also shown promising outcomes as a hemocompatible material (Ref 17-19). Various studies reported that the DCC is a biocompatible material which is a good alternative to existing materials used in biomedical implants (Ref 20-22). However, to the best of our knowledge, until now there are no studies reported on the corrosion behavior of the DCC on specifying an exact combination of titanium alloys.

In this work, Ti-6Al-4V and Ti-13Nb-13Zr alloys were selected for the investigation. Ti-6Al-4V is $\alpha + \beta$ alloy type which possesses excellent resistance toward corrosion and provides a unique biocompatibility. Moreover, it is still under the investigation because of the hazardous nature of vanadium. Ti-13Nb-13Zr is near-β-type titanium alloy which has low modulus and good biocompatibility, as well as approved by Food and Drug Administration (FDA), USA. Besides, it was found that the titanium compounds offer great grip diamond (Ref 23). Hot filament chemical vapor deposition (HFCVD) is a standout among the most generally perceived methods for the deposition of diamond carbon on the different substrate and furthermore easy to create uniform precious diamond carbon coating over a large surface (Ref 24). In this present work, the corrosion and the electrical impedance characteristics of DCC on Ti-6Al-4V (ASTM grade 5) and Ti-13Nb-13Zr (ASTM F1713-08) are examined in detail.

2. Materials and Methods

2.1 Sample Preparation

Initially, a test sample of titanium alloys of 2 mm thickness was cut into regular square-shaped pieces (10 mm × 10 mm). The cut pieces were grounded using silicon carbide paper with the range of 200-1600# grits and polished with the use of diamond paste (0.4 microns). The polished samples were placed in an ultrasonicator and cleaned with ethanol followed by the HNO_3 (nitric acid) treatment for 5 min to remove the oxide layer present over the substrate (titanium alloys).

2.2 Deposition System

Before diamond deposition, the substrates were seeded with diamond nanoparticle (∼ 6 nm diameter), dispersed in dimethyl sulfoxide (DMSO), using ultrasonicator for 30 min. The titanium substrates again cleaned with ethanol in an ultrasonicator for 2 min. The samples were placed in the cold walled aluminum chamber of HFCVD systems (SP3 diamond technology, USA). An array of parallel wires of (0.12 mm) diameter filaments with 12-mm wire-to-wire spacing and standoff distance 19 mm was placed above the samples. The HFCVD chamber pressure was controlled using throttle valve connected to the rotary pump. Flow rates of the precursor gases such as CH_4 (45 sccm) and H_2 (2250 sccm) were maintained by mass flow controller in the range of 10-90% accuracy (MKS Instrument, USA). The chamber pressure during the deposition was set to 10 Torr and controlled by a throttle valve connected to a rotary pump. A two-color optical pyrometer was used to monitor the tungsten filament temperature (∼ 2200 °C). The substrates temperature was measured using K-type thermocouple located at the bottom of the titanium substrates. The substrates were found to be 800 °C. The whole deposition process was performed for 2 h, and the coating thickness of the film estimated to be ∼ 1 μm (Ref 25).

2.3 Characterization Technique

The surface morphological experiments were carried out using field emission scanning electron microscopy (FESEM) supplied by Carl Zeiss, Germany supra 40VP FESEM. Buehler micro-Vickers's hardness tester was used to measure the microhardness of the substrate. Nd: YAG laser source with the wavelength of 532 nm used for Raman analysis supplied by LABRUM 010, UK. The topographical study was carried out using atomic force microscopy (AFM) with Easy scan2 supplied by Nanosurf, Switzerland.

2.4 Electrochemical Measurement

CHI604D electrochemical workstation provided by CH Instruments, USA, was used for electrochemical studies on substrates and coated samples. The chemical composition of SBF is tabulated in Table 1. The pH of SBF solution (7.2-7.5) was balanced by one molar hydrochloric acid solution. The test was carried out in 400 ml of SBF solution at 36 ± 1 °C. The substrate was used as the working electrode; and the counter electrodes are platinum foil and saturated calomel electrode (SCE), respectively. A luggin capillary was connected to SCE electrode, and the capillary tip was placed very close to the working electrode surface. The samples were immersed in the Hanks' solution for an hour to create the open circuit potential (OCP) or steady-state potential. The electrochemical impedance spectroscopy (EIS) for the sample (Ti alloys) was tested within the frequency range between 100 kHz and 10 MHz. 10 mV of AC (alternating current) was applied on open circuit potential. Nyquist and Bode plots were obtained from the impedance data for each test. After EIS measurements, the system was permitted to achieve open circuit potential (OCP); then the

Table 1 SBF preparation

Order	Reagent	Amount, g
1.	$CaCl_2$	0.185
2.	KCl	0.4
3.	KH_2PO_4	0.06
4.	$MgCl_2{\cdot}6H_2O$	0.1
5.	$MgSO4{\cdot}7H_2O$	0.1
6.	$NaCl_2$	8
7.	$NaHCO_3$	0.35
8.	Na_2HPO_4	0.48
9	D-Glucose	1

electrode was linearly polarized from an initial potential of 200 mV below the OCP value to 200 mV on the positive side at one mV/s of scan rate. The measured current and potential data were used to plot Tafel plots. Tafel plots are drawn between potential and log (i) plot. Therefore, with the help of the Tafel plot, E_{corr}—(the corrosion potential) and I_{corr}—(the corrosion current) were concluded. Stern–Geary equation (Ref 26, 27) is used to determine corrosion current.

$$I_{corr} = (\beta a \times \beta c)/2.3\mathrm{Rp}\ (\beta a + \beta c) \qquad \text{(Eq 1)}$$

where βa and βc—slopes of the anodic and cathodic parts of the Tafel Plot, R_p—polarization resistance.

3. Results and Discussion

3.1 Raman Analysis

The DCC is the combination of sp^3 and sp^2 hybridized bonds. The tribological outcome of DCC coating combination strongly depends on a function of bonding ratio, i.e., sp^2/sp^3. This bonding ratio is characterized using Raman spectroscopy in which relative peaks of *D* and *G* of I_D/I_G play a vital role in Raman studies (Ref 28, 29). Thus, in determining the quality of diamond carbon-coated surface, the bonding ratio (sp^3/sp^2) is considered to be the predominant factor. The Raman spectra were recorded in the wave number ranging from 1000 to 1800 cm^{-1}. Micro-Raman spectra of DCC coatings consist of disorder (*D*) and graphite (*G*) peaks. From Fig. 1 the peak at 1319 cm^{-1} is attributed to diamond and peak at 1476 cm^{-1} belongs to single graphite. The *G* band centered around 1450-1700 cm^{-1} which relates to sp^2 characteristics of graphite-like materials. On the other hand, *D* band centered around 1200-1400 cm^{-1} relates to sp^2 graphite bond angle disorder which may occur due to breathing mode of a sp^3 carbon atom, and also the crystalline size in sp^2 domains (Ref 30).

The intensity ratio of *D* and *G* (I_D/I_G) is a parameter of relative quantities of sp^3/sp^2 bonds. The intensity ratio I_D/I_G was calculated, and it was found to be 1.397 for diamond carbon-coated Ti-13Nb-13Zr alloy and 1.131 for diamond carbon-coated Ti-6Al-4V alloy. These results demonstrate that the intensity ratio of the Ti-13Nb-13Zr alloy is higher than that of Ti-6Al-4V. Increased I_D/I_G ratio is due to the increased amount of sp^3 bond in the coated substrate (Ref 30). Thus, the surface becomes smoother when an exchange of graphite film frames on the counter surface. The smaller increase in the I_D/I_G ratio enhances the graphitization of the coated material. Hence, the surface becomes smoother when a transfer of graphite film forms on the counter surface.

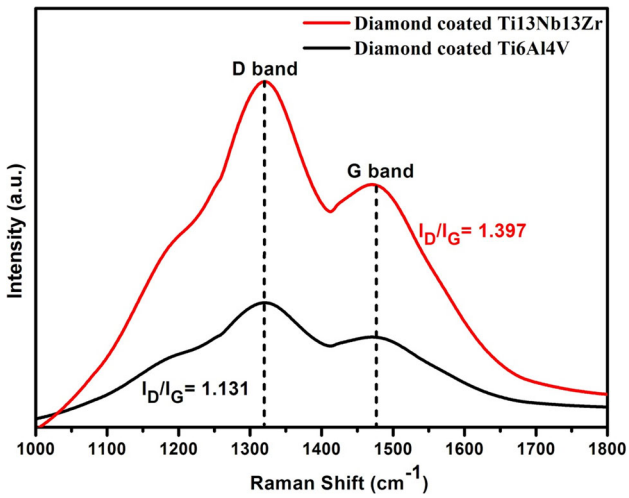

Fig. 1 Raman spectra of diamond carbon-coated Ti-6Al-4V and Ti-13Nb-13Zr substrates

3.2 Surface Morphology

The FESEM image of diamond carbon-coated Ti-6Al-4V and Ti-13Nb-13Zr substrates is shown in Fig. 2. From the FESEM micrograph, continuous and well-faceted diamond carbon crystals are identified. The calculated particle sizes of the DCC on the Ti-6Al-4V and Ti-13Nb-13Zr alloys are ~ 250 and ~ 80 nm, respectively. The larger grain size of the Ti-13Nb-13Zr alloy was attributed to the great seeding of diamond on the β phase. The enhanced subsequent growth of diamond on the β phase Ti-13Nb-13Zr metal results in bulk grain size. However, α-β titanium alloy has a different atom arrangement in the crystal plane such as hcc (α) and bcc (β) structure. The nucleation rate of the diamond carbon-coated α-β titanium alloy is very less, and hence, the growth factor is predicted to be hidden (Ref 31).

Atomic force microscopy (AFM) was used to analyze the surface topography of the diamond carbon-coated titanium alloys (Ti-6Al-4V and Ti-13Nb-13Zr), and the images are shown in Fig. 3. It is observed from the analysis that the DCC-coated Ti-6Al-4V alloy showed an estimated surface roughness (Ra) of 157 nm and root mean square (RMS) value of 598 nm. Similarly, DCC Ti-13Nb-13Zr alloy showed the Ra and RMS as 136 nm and 1114 nm, respectively. The surface roughness value of the diamond carbon-coated near-β titanium alloy is superior to that of the α-β titanium alloy. Hence, the larger grain size is assigned to diamond carbon-coated near-β titanium alloy (Ref 32).

Figure 4 shows the microhardness of the coated and uncoated titanium alloys samples (Ti-6Al-4V and Ti-13Nb-13Zr) at different applied loads (500, 1000, 1500 and 2000 gf). It is noticed that the diamond carbon-coated Ti-6Al-4V and Ti-13Nb-13Zr alloys showed greater hardness when compared to uncoated alloys (Ti-6Al-4V and Ti-13Nb-13Zr). The surface hardness of diamond carbon-coated Ti-13Nb-13Zr alloys is found to be relatively higher when compared to the Ti-6Al-4V alloy. It is clear that the hardness of DCC titanium alloys depends on the crystallinity and coating thickness (Ref 33). The increase in hardness of DCC near β titanium alloys enhances the wear properties of the implants.

3.3 In vitro Electrochemical Studies

To understand the corrosion behavior of diamond carbon coatings over Ti-6Al-4V and Ti-13Nb-13Zr, electrochemical studies were conducted. The potentiodynamic polarization curves obtained for the bare substrates and diamond carbon-coated substrates in simulated body fluids solution (SBF) are presented in Fig. 5. Using Eq. 1, the corrosion current (I_{corr}) density obtained by extrapolating the cathodic and anodic branches of polarization curves (Ref 34). Table 2 gives the corrosion current densities and corrosion potential (E_{corr}) for different substrates used in the present study. The corrosion current density (I_{corr}) is 4.5×10^{-8} μA/cm^2 for the Ti-6Al-4V substrate and 7.41×10^{-9} μA/cm^2 for diamond carbon-de-

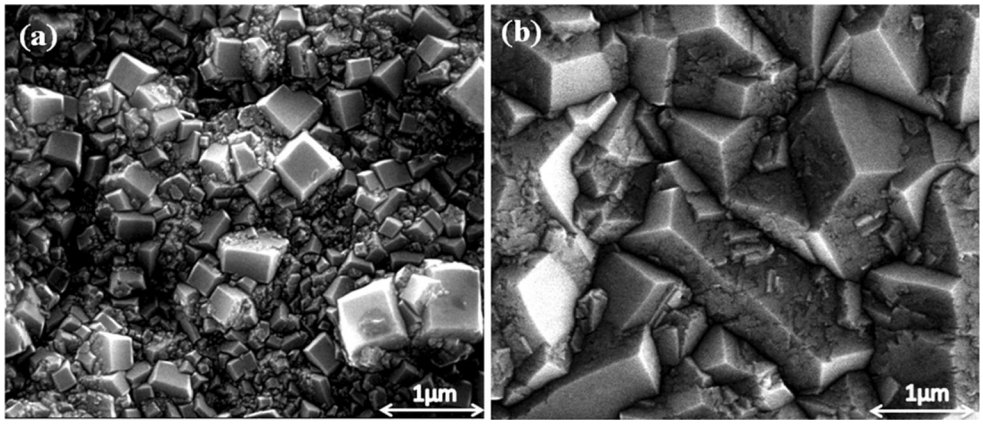

Fig. 2 SEM images of diamond carbon-coated metal alloys (a) Ti-6Al-4V and (b) Ti-13Nb-13Zr

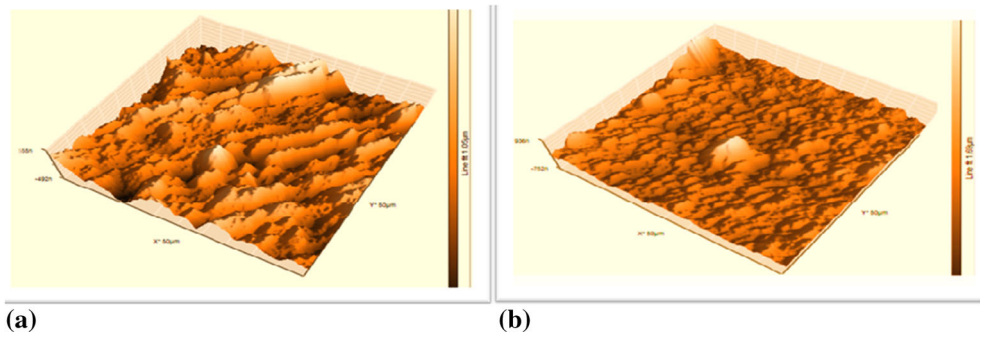

Fig. 3 Surface topography obtained from AFM for diamond carbon-coated alloys (a) Ti-6Al-4V and (b) Ti-13Nb-13Zr

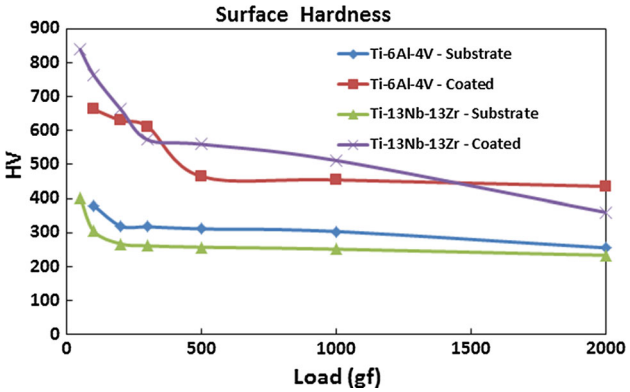

Fig. 4 Microhardness of diamond carbon-coated and uncoated titanium (Ti-6Al-4V and Ti-13Nb-13Zr) alloys

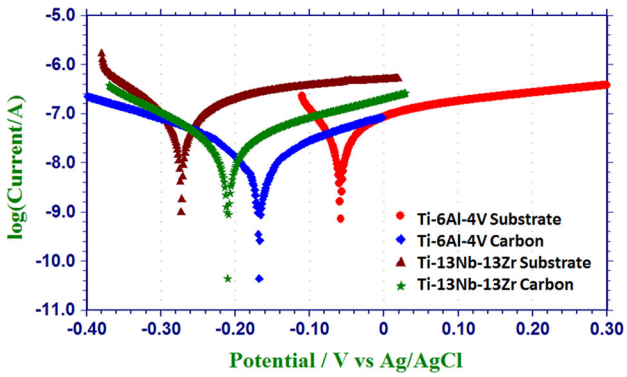

Fig. 5 Potentiodynamic polarization curves for diamond carbon-coated and uncoated titanium (Ti-6Al-4V and Ti-13Nb-13Zr) alloys

posited Ti-6Al-4V. The corrosion current density is 3.09×10^{-8} µA/cm^2 for Ti-13Nb-13Zr substrate and 3.80×10^{-9} µA/cm^2 for DCC Ti-13Nb-13Zr alloy. Hence, the corrosion resistance of the substrates increased gradually after surface modification.

The E_{corr} value of diamond carbon-coated Ti-6Al-4V alloys tends to active region with the value of − 0.168 V compared to bare substrate − 0.057 V. On the other hand, diamond carbon-coated Ti-13Nb-13Zr showed more noble value (− 0.210 V) when compared to bare substrate (− 0.273 V). This behavior could be due to the difference in formation of coating on different substrate materials. The results of electrochemical impedance test in Hanks' solution are presented Fig. 6(a) and (b) in the form of Bode plots and Fig. 6(c) in the form of Nyquist plots. For Ti-6Al-4V substrate (see Fig. 6a), the phase angle changes from − 25° to − 10° in high frequency range (10-100 kHz). At low frequency range from 0.1 to 100 Hz, the phase angle around − 78° was remained as nearly constant ($< -90°$) which is valuable for an ideal capacitor. At 0.1-0.01 Hz (very low frequencies), the phase angle gradually changed to − 60°. On the other hand, for Ti-13Nb-13Zr substrate [see Fig. 6(a)], the phase angle varies rapidly between − 40° and − 10° in the frequency range from 10 to 100 kHz. At low frequency range between 0.01 and 100 Hz, the phase angle around − 82° was remained as nearly constant. A linear relationship for log $|z|$ and log f is obtained with a slope close to

Table 2 Potentiodynamic polarization results of substrate and coated samples

S. no	Sample	E_{corr}, V	I_{corr}, μA/cm^2
1.	Ti-6Al-4V substrate	− 0.057	4.57×10^{-8}
2.	Ti-6Al-4V diamond carbon-coated	− 0.168	7.41×10^{-9}
3.	Ti-13Nb-13Zr substrate	− 0.273	3.09×10^{-8}
4.	Ti-13Nb-13Zr diamond carbon-coated	− 0.210	3.80×10^{-9}

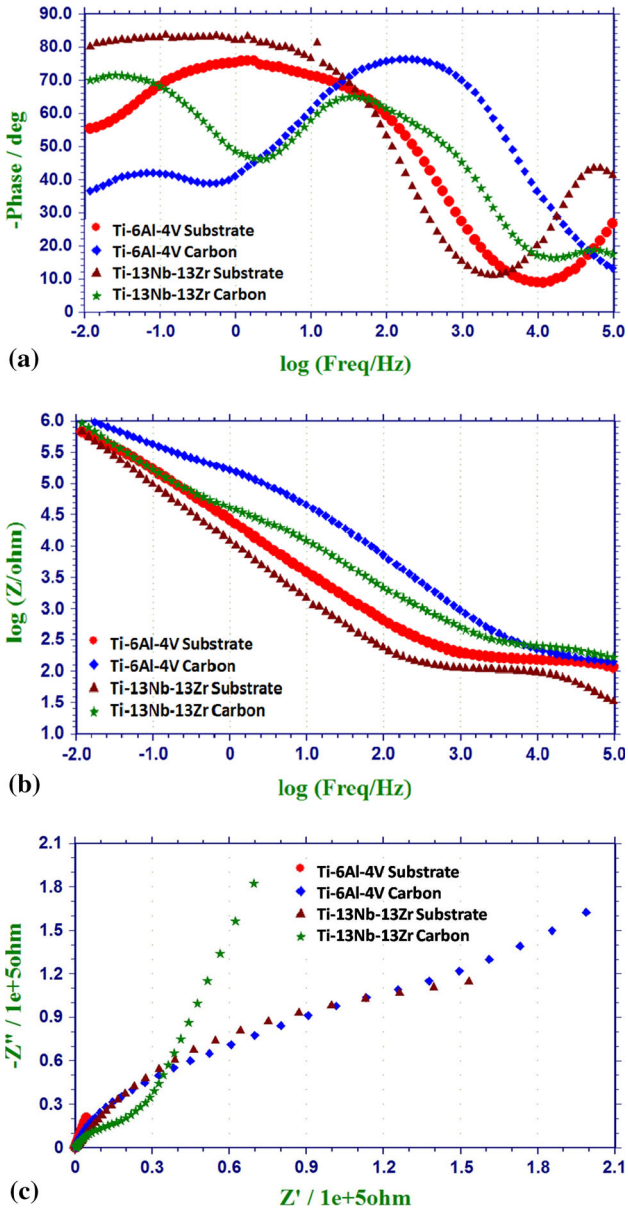

Fig. 6 Bode plots obtained in Hanks' solution: (a) phase, (b) magnitude and (c) Nyquist plots of coated and uncoated substrates

one in the same frequency range in Fig. 6(b). In Fig. 6(a), for Ti-6Al-4V diamond carbon-coated samples, the phase angle rapidly changes from − 10° to − 75° in the high frequency range (100 Hz to 100 kHz). Between 100 and 1 Hz frequency range, a sudden fall in the phase angle to − 40° is noticed. In the case of Ti-13Nb- 13Zr diamond carbon-coated samples, the phase angle changes from − 20° to − 60° in the high frequency range (100 Hz to 100 kHz). Between 100 and

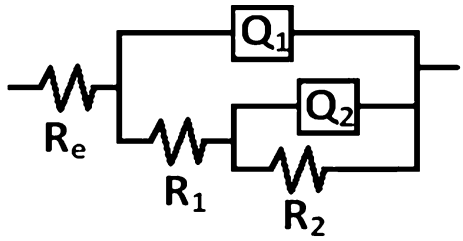

Fig. 7 Equivalent circuit (EC) diagram used for fitting EIS data of the substrate and diamond carbon-coated samples

1 Hz frequency range, a sudden fall in the phase angle to − 40° is noticed. In the very low frequency range between 1 and 0.01 Hz, the phase angle increases rapidly to − 70°. The Nyquist plots of DCC samples in Fig. 6(c) showed a larger diameter at higher frequencies when compared to uncoated substrates.

The electrochemical equivalent circuit (EEC) model which is used to fit the EIS (electrochemical impedance spectroscopy) data for pure DCC substrate and uncoated substrate as shown in Fig. 7. The EEC consists of resistances and CPE (constant phase element). This CPE is used to change in the relaxation times as a result of different degrees of surface inhomogeneity. The impedance with the capacitance can be defined as $Z_{CPE} = [Q\ (j\omega^n)]^{-1}$, where Q, j, ω and n are the pseudo-capacitance or non-ideal capacitance, imaginary function ($\sqrt{-1}$), angular frequency and the deviation from the ideal behavior of a pure capacitor, respectively. When $n = 1$, the system behaves like a pure capacitor and $Q = C$, where C is capacitance (Ref 35, 36). In the EEC the resistive component R_s represents the solution resistance. R_1 and R_2 represent outer and inner layer resistances, respectively. Q_1 and Q_2 represent the capacitance of the outer layer and inner layer, respectively. The parameters Q_1 and R_1 represent properties of the porous film/solution interface, i.e., the charge transfer resistance and double layer capacitance. Table 3 gives the electrical parameter values obtained by fitting the EIS data for the substrate and DCC-coated samples. From Table 3, uncoated substrate (Ti-6Al-4V and Ti-13Nb-13Zr) of the inner oxide layer corrosion resistance R_2 is 2.77×10^6 and $6.98 \times 10^6\ \Omega\,cm^2$, respectively. The substrate (Ti-6Al-4VTi-6Al-4V and Ti-13Nb-13Zr) outer porous layer resistance is 106 and $90\ \Omega\,cm^2$, respectively. The CPE value of n_1 outer layer substrate is 0.78 and 0.93 (Ti-6Al-4V and Ti-13Nb-13Zr), and the inner layer n_2 substrate is 0.91 and 0.90 (Ti-6Al-4V and Ti-13Nb-13Zr). The non-ideal value for the CPE value of n_1 outer layer DCC is 0.78 and 0.73 (Ti-6Al-4V and Ti-13Nb-13Zr), and inner layer n_2 DCC is 0.90 and 0.92 (Ti-6Al-4V and Ti-13Nb-13Zr) which is very close to unity when compared to the uncoated titanium alloys. The results indicate that protection provided by passive layer is predominately due to the barrier layer (Ref 36). Hence, the diamond carbon-coated titanium alloys are observed to be a

Table 3 Equivalent circuit parameters obtained by fitting the electrochemical impedance data for substrates and diamond coated samples

Sample	Re, Ω cm^2	Q_1 S s^n, 1/cm^2	n_1	R_1, Ω cm^2	Q2 S s^n, 1/cm^2	n_2	R_2, Ω cm^2	χ^2
Ti-6Al-4V substrate	14	2.62×10^{-6}	0.78	106	5.95×10^{-6}	0.91	2.77×10^{6}	8.7×10^{-4}
Ti-6Al-4V diamond carbon-coated	15	5.35×10^{-7}	0.78	1.49×10^{5}	3.38×10^{-6}	0.90	3.56×10^{6}	5.6×10^{-4}
Ti-13Nb-13Zr substrate	16	1.60×10^{-5}	0.93	90	1.67×10^{-7}	0.90	6.98×10^{6}	3.6×10^{-4}
Ti-13Nb-13Zr diamond carbon-coated	20	4.70×10^{-6}	0.73	3.31×10^{5}	1.14×10^{-6}	0.92	9.42×10^{6}	1.8×10^{-3}

good choice due to its better electrochemical reactions, enhanced surface hardness and corrosion resistance properties.

4. Conclusion

Diamond carbon has been deposited on Ti-13Nb-13Zr and Ti-6Al-4V biomedical alloy by HFCVD method. The FESEM results show that diamond carbon-coated Ti-13Nb-13Zr particle size is greater than the diamond carbon-coated Ti-6Al-4V sample. Raman studies confirmed the formation of diamond carbon crystal coatings. The surface hardness of the diamond carbon-coated Ti-13Nb-13Zr alloy is higher than the diamond carbon-coated Ti-6Al-4 V alloy, which leads to improved mechanical properties of the implants. Potentiodynamic polarization studies showed that the corrosion resistance of diamond carbon-coated Ti-13Nb-13Zr alloy is better than the bare Ti-6Al-4V. Electrochemical impedance studies in SBF solution showed that diamond carbon-coated samples behave like a near-ideal capacitor with better passivation behavior than the bare substrates. The polarization resistance and corrosion current density of the diamond carbon-coated Ti-13Nb-13Zr alloy is relatively higher when compared to the diamond carbon-coated Ti-6Al-4V substrate. Hence, diamond carbon-coated Ti-13Nb-13Zr alloy helps in improving the corrosion and mechanical properties. Therefore, diamond carbon-coated near-β titanium alloy provides higher corrosion protection and also offers good mechanical properties than that of the diamond carbon-coated Ti-6Al-4V alloy, which can be used for biomedical implant applications.

References

1. S. Kurtz, Projection of Primary and Revision Hip and Knee Arthoroplasty in Unites State from 2005 to 2030, *J. Bone Jt. Surg.*, 2007, **89**, p 780–785
2. S.M. Kurtz, E. Lau, K. Ong, K. Zhao, M. Kelly, and K.J. Bozic, Future Young Patient Demand for Primary and Revision Joint Replacement: National Projections from 2010 to 2030, *Clin. Orthop. Relat. Res.*, 2009, **467**, p 2606–2612
3. M. Geetha, A.K. Singh, R. Asokamani, and A.K. Gogia, Ti Based Biomaterials, the Ultimate Choice for Orthopedic Implants, *Prog. Mater. Sci.*, 2009, **54**, p 397–425
4. M. Long and H.J. Rack, Titanium Alloys in Total Joint Replacement—A Materials Science Perspective, *Biomaterials*, 1998, **19**, p 1621–1639
5. Y. Abu-Amer, I. Darwech, and J.C. Clohisy, Aseptic Loosening of Total Joint Replacements: Mechanisms Underlying Osteolysis and Potential Therapies, *Arthritis Res. Ther.*, 2007, **9**, p S6
6. R. Pareta, L. Yang, A. Kothari, S. Sirinrath, X. Xiao, B.W. Sheldon et al., Tailoring Nanocrystalline Diamond Coated on Titanium for Osteoblast Adhesion, *J. Biomed. Mater. Res. Part A*, 2010, **95**, p 129–136
7. Y. Yan, A. Neville, and D. Dowson, Bio Tribocorrosion of Co Cr Mo Orthopedic Implant Materials—Assessing the Formation and Effect of the Biofilm, *Tribol. Int.*, 2007, **40**, p 1492–1499
8. R. Hauert, *Tribology of Diamond-like Carbon Films: Fundamentals and Applications*, ed by C. Donnet, A. Erdemir (Springer, New York, 2008) pp. 494–509
9. X. Liu, P.K. Chu, and C. Ding, Surface Nano-functionalization of Biomaterials, *Mater. Sci. Eng.*, 2010, **70**(3–6), p 275–302
10. V. Gopal, M. Chandran, and M.S. Ramachandra, Tribocorrosion and Electrochemical Behaviour of Nanocrystalline Diamond Coated Ti Based Alloys for Orthopaedic Application, *Tribol. Int.*, 2017, **106**, p 88–100
11. S.P. Patterson, R.H. Daffner, and R.A. Gallo, Electrochemical Corrosion of Metal Implants, *AJR Am. J. Roentgenol.*, 2005, **184**, p 1219–1222
12. S.R. Paital and N.B. Dahotre, Calcium Phosphate Coatings for Bio-implant Applications: Materials, Performance Factors, and Methodologies, *Mater. Sci. Eng.*, 2009, **66**, p 1–3
13. M. Spector, Biomaterial Failure, *Orthop. Clin.*, 1992, **23**, p 211–217
14. M. Kaczmare, M.U. Jurczyk, A. Miklaszewski, A. Paszel-Jaworska et al., In Vitro Biocompatibility of Titanium After Plasma Surface Alloying with Boron, *Mater. Sci. Eng. C*, 2016, **69**, p 1240–1247
15. R. Hauert, A Review of Modified DLC Coatings for Biological Applications, *Diamond Relat. Mater.*, 2003, **12**, p 583–589
16. A. Grill, Tribology of Diamond Like Carbon and Related Materials: An Updated Review, *Surf. Coat. Technol.*, 1997, **94**, p 507–513
17. P. Yang, S.C.H. Kwok, P.K. Chu, Y.X. Leng, J.Y. Chen, J. Wang, and N. Huang, Haemocompatibility of Hydrogenated Amorphous Carbon (a-C:H) Films Synthesized by Plasma Immersion Ion Implantation-Deposition, *Nucl. Instrum. Methods Phys. Res. Sect. B*, 2003, **206**, p 721–725
18. L.J. Yu, X. Wang, X.H. Wang, and X.H. Liu, Heamo Compatibility of Tetrahedral Amorphous Carbon Film, *Surf. Coat. Technol.*, 2000, **128**(129), p 484–488
19. N. Urdin, P. Francois, M. Moret, K. Unal, J. Krumeich, B.O. Aronsson, and P. Descounts, Hemocompatible Diamond-Like Carbon (DLC) Surfaces, *Eur. Cells Mater.*, 2003, **5**, p 17–28
20. M.I. Jones, I.R. McColl, D.M. Grant, K.G. Parker, and T.L. Parker, Haemocompatibility of DLC and TiC–TiN Interlayers on Titanium, *Diamond Relat. Mater.*, 1999, **8**(2–5), p 457–462
21. S. Linder, W. Pinkowski, and M. Aepfelbacher, Adhesio Cytoskeletal Architecture and Activation Status of Primary Human Macrophages on a Diamond-Like Carbon Coated Surface, *Biomaterials*, 2002, **23**, p 767–773
22. K. Al Mahmud, M. Varman, M. Kalam, H. Masjuki, H. Mobarak, and N. Zulkifli, Tribological Characteristics of Amorphous Hydrogenated (aC: H) and Tetrahedral (ta-C) Diamond-Like Carbon Coating at Different Test Temperatures in the Presence of Commercial Lubricating Oil, *Surf. Coat. Technol.*, 2014, **245**, p 133–147
23. M. Mohanty, T.V. Anilkumar, P.V. Mohanan, C.V. Muraleedharan, G.S. Bhuvaneshwar, F. Derangere, Y. Sampeur, and R. Suryanarayanan, Long Term Tissue Response to Titanium Coated with Diamond Like Carbon, *Biomol. Eng.*, 2002, **19**, p 125–128
24. D. Sheeja, B.K. Tay, and L.N. Nung, Feasibility of Diamond-Like Carbon Coatings for Orthopedic Applications, *Diamond Relat. Mater.*, 2004, **13**(1), p 184–190
25. S.H. Din, M.A. Shah, and N.A. Sheikh, Effect of CVD-Diamond on the Tribological and Mechanical Performance of Titanium Alloy (Ti6Al4V), *Tribol. Ind.*, 2016, **38**(4), p 530–542
26. L. Mohan, P. Dillibabu, P. Kmar, and C. Anandan, Influence of Zirconium Doping on the Growth of Apatite and Corrosion Behavior

of DLC-Coated Titanium Alloy Ti-13Nb-13Zr, *Surf. Interface Anal.*, 2013, **45**(11–12), p 1785–1791

27. V. Baranauskas, H.J. Ceragioli, A.C. Peterlevitz, and M. Fontana, Low Residual Stress Diamond Coatings on Titanium, *Surf. Coat. Technol.*, 2005, **200**, p 2343–2347
28. S. Ghosh, D. Choudhury, T. Roy, A.B. Mama, H.H. Masjuki, and B. Pingguan-Murphy, Tribological Investigation of Diamond Like Carbon Coated Micro-dimpled Surface Under Bovine Serum and Osteoarthritis Oriented Synovial Fluid, *Sci. Technol. Adv. Mater.*, 2015, **16**, p 3
29. S. Tamilselvi, V. Raman, and N. Rajendran, Electrochemical Impedance Spectroscopic Characterization of Titanium During Alkali Treatment and Apatite Growth in Simulated Body Fluid, *Electrochem. Acta*, 2007, **52**, p 7418–7424
30. T. Falcade, T.E. Shimitzhauz, O.G. dos Reisb et al., Electrodeposition of Diamond-Like Carbon Films on Titanium Alloy Using Organic Liquids: Corrosion and Wear Resistance, *Appl. Surf. Sci.*, 2012, **263**, p 18–24
31. T.J. Dines, D. Tither, A. Dehbi, and A. Mathews, Raman Spectra of Hard Carbon Films and Hard Carbon Films Containing Secondary Elements, *Carbon*, 1991, **29**, p 225–231
32. D. Durgalakshmi and M. Chandran, Studies on Corrosion and Wear Behavior of Sub Micrometric Diamond Coated Ti Alloys, *Tribol. Int.*, 2013, **63**, p 132–140
33. B. Ramamoorthy, B.C. Yelldose, and Scires, An Investigation into the Adhesion Strength of Diamond Like Carbon Multilayer Coating (DLC/TiN/Ti/Cu/Ni), *IIM Int.*, 2009, **1**, p 179–194
34. C. Anandan and L. Mohan, Wear and Corrosion Behavior of Oxygen Implanted Biomedical Titanium Alloy Ti-13Nb-13Zr, *Appl. Surf. Sci.*, 2013, **282**, p 281–290
35. M. Metikos-Hukovic and R. Babic, Passivation and Corrosion Behaviours of Cobalt and Cobalt–Chromium–Molybdenum Alloy, *Corros. Sci.*, 2007, **40**, p 3570–3579
36. I. Milosev, T. Kosec, and H.H. Strehblow, XPS and EIS Study of the Passive Film Formed on Orthopaedic Ti-6Al-7Nb Alloy in Hank's Physiological Solution, *Electrochim. Acta*, 2008, **53**, p 3547–3558